Technical Note

1966-47

S. D. Wiener

A Model of Radar Scattering from the Cone-Sphere

20 October 1966

Prepared for the Advanced Research Projects Agency
under Electronic Systems Division Contract AF 19(628)-5167 by

Lincoln Laboratory

MASSACHUSETTS INSTITUTE OF TECHNOLOGY

Lexington, Massachusetts

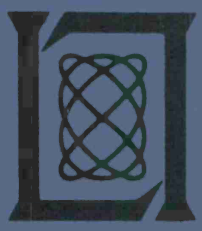

The work reported in this document was performed at Lincoln Laboratory, a center for research operated by Massachusetts Institute of Technology. This research is a part of Project DEFENDER, which is sponsored by the U.S. Advanced Research Projects Agency of the Department of Defense; it is supported by ARPA under Air Force Contract AF 19(628)-5167 (ARPA Order 498).

MASSACHUSETTS INSTITUTE OF TECHNOLOGY

LINCOLN LABORATORY

A MODEL OF RADAR SCATTERING FROM THE CONE-SPHERE

S. D. WEINER

Group 41

TECHNICAL NOTE 1966-47

20 OCTOBER 1966

LEXINGTON MASSACHUSETTS

Abstract

A technique is presented for calculating the radar cross section of a conducting cone-sphere as a function of cone angle, aspect angle, tip radius, base radius, and wavelength for both cw and short-pulse incident signals. A modification of the physical optics approximation is used in which the incident sinusoidal wave is replaced by a pulse of triangular waves, permitting the physical optics integrals to be replaced by finite summations. Creeping waves are included by using the known results for a sphere combined with an aspect-angle dependence obtained from a ray-tracing model. For long incident pulses, the calculated cross sections show good agreement with cw measured values. For short incident pulses, the behavior of individual scattering centers may be studied as a function of the target parameters.

Accepted for the Air Force
Franklin C. Hudson
Chief, Lincoln Laboratory Office

A Model of Radar Scattering from the Cone-Sphere

I. INTRODUCTION

There are only a few target shapes for which electromagnetic scattering is exactly calculable and as a consequence, many approximation techniques have been developed. One of the most widely used of these is the physical optics or Kirchoff approximation.[1] The basic assumption of this method is that the surface current at a point on the target is the same as would be produced on an infinite plane tangent to the target at that point. There are several variations of physical optics which differ in their treatment of shadow regions and shadow boundaries, but all of these retain the basic assumption mentioned above. This assumption appears to restrict the validity of physical optics to targets with characteristic dimensions (such as radii of curvature) large compared with a wavelength. However, there are cases for which physical optics is applicable for bodies with small characteristic dimensions. For both pointed and rounded cone tips, it has been shown[2] that the physical optics results closely approximate results obtained from a more exact theory.

Even though physical optics represents a considerable simplification of electromagnetic theory, in many cases the physical optics integrals must be evaluated either numerically or by means of some analytic approximation. In the following sections we will use an approximate waveform for the incident signal, which considerably simplifies the physical optics calculations. The agreement between these results and more exact (theoretical and experimental) results will then be used to justify applying the present model to cases which have not been considered previously.

The present model will be applied to calculate both the cw and short-pulse scattering of cone-spheres at all aspect angles. The scattering from these targets is generally expressed in terms of returns from various scattering centers. Depending on the aspect angle, these may include tip, joint, specular, and creeping-wave returns. The tip, joint, and specular returns are

fairly well approximated by physical optics. At zero aspect angle (nose-on), the creeping-wave return is closely approximated by the creeping-wave return for an isolated sphere. A simple model is used to estimate the creeping-wave return at non-zero aspect angles. The results obtained by combining physical optics and the creeping-wave model show agreement with cw measurements. The predicted short-pulse results may be used to estimate the contribution of the various scattering centers as functions of aspect angle, wavelength, etc.

II. PHYSICAL OPTICS FOR TRANSIENT SIGNALS

Most work in electromagnetic scattering has been concerned with the response of a target to an infinite sinusoidal incident wave. In this case, the back-scattered magnetic field is given by[1]

$$\vec{H}_s = \hat{\epsilon} \frac{ikH_o}{2\pi r} \exp(-ikr) \int_S \exp(-2ikz) \frac{dA}{dz} \, dz \quad , \tag{2.1}$$

where k, H_o, and $\hat{\epsilon}$ are the wave number, amplitude, and unit polarization vector of the incident field, r is the distance to the observation point, A is the area of the target intersecting a plane of constant z, and S is usually taken to be the illuminated surface of the target. In Eq. (2.1), z is taken along the direction of incidence (not necessarily the symmetry axis of the body) and, in general, the integral is quite complicated. For transient incident signals, we must take the Fourier transform of Eq. (2.1) weighted by the incident spectrum, $H_o(k)$. We then obtain

$$\vec{H}_s(\vec{r}, t) = \frac{\hat{\epsilon}}{2\pi r} \int_{-\infty}^{\infty} dk \, ikH_o(k) \exp[-ik(r - ct + 2z)] \int_S \frac{dA}{dz} \, dz \quad . \tag{2.2}$$

Performing the k integration first, we are left with

$$H_s(r - ct) = \frac{\hat{\epsilon}}{2\pi r} \int_S H_o'(r - ct + 2z) \frac{dA}{dz} \, dz \quad , \tag{2.3}$$

where H_o' is the derivative of the incident waveform.

For the particular cases of impulse, step, and ramp waveforms, the integral in Eq. (2.3) is trivial, giving d^2A/dz^2, dA/dz, and A respectively

(evaluated at $2z = ct - r$). Kennaugh and co-workers[3,4] have considered the impulse response of several bodies in some detail. However, they have modified the physical optics approximation to improve their long-wavelength results. In the present discussion, we will be concerned with the short-wavelength response of a cone-sphere and will modify physical optics only to include creeping waves.

There are several disadvantages in the use of the impulse response. Perhaps the most serious drawback is that the impulse is a poor representation of any physical waveform. The impulse has a non-zero dc component and is not capable of indicating the wavelength dependence of scattering. These latter two objections may be removed by combining positive and negative impulses separated by half a wavelength. However, the resulting waveform is still not physically reasonable. Other waveforms may be formed by appropriately combining step or ramp functions. For our purposes, we will use a pulse of triangular waves formed from ramp functions, as shown in Fig. 1. Use of such a waveform simplifies the calculations considerably and provides a fairly good approximation to a pulsed sinusoid. The Fourier expansion of this waveform contains only odd harmonics with the amplitude of the nth harmonic decreasing as $1/n^2$. If we consider a pulse one wavelength long, the resulting field is expressed in terms of the ramp response as follows:

$$\text{Field}(z) = \text{Ramp}(z) - 2\text{Ramp}(z - \lambda/8) + 2\text{Ramp}(z - 3\lambda/8) - \text{Ramp}(z - \lambda/2) \quad , \tag{2.4}$$

where $z = (ct - r)/2$. Thus, the physical optics integrals have been approximated by finite sums. From Eq. (2.3), we find the ramp response to be

$$\text{Ramp}(z) = \frac{\hat{\epsilon}}{2\pi r} A(z) \quad , \tag{2.5}$$

which is easily calculated.

Examination of Eq. (2.4) gives some insight into the results to be expected. After some algebra, the scattered field is seen to be proportional to the third finite difference of the ramp response (or the target area). In the limit of small wavelength, the scattering from the target is localized in those

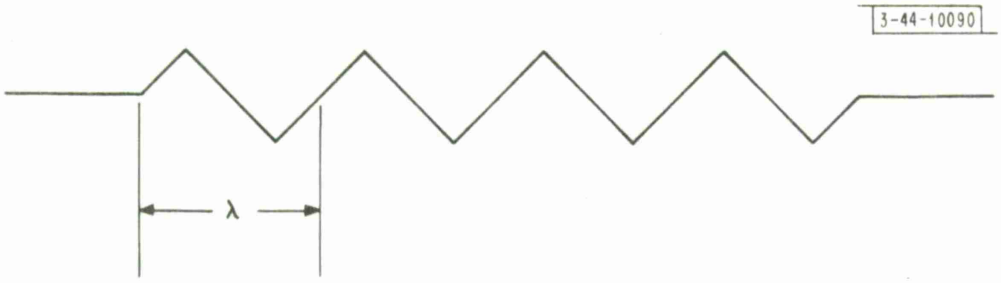

Fig. 1. Pulse constructed from ramps.

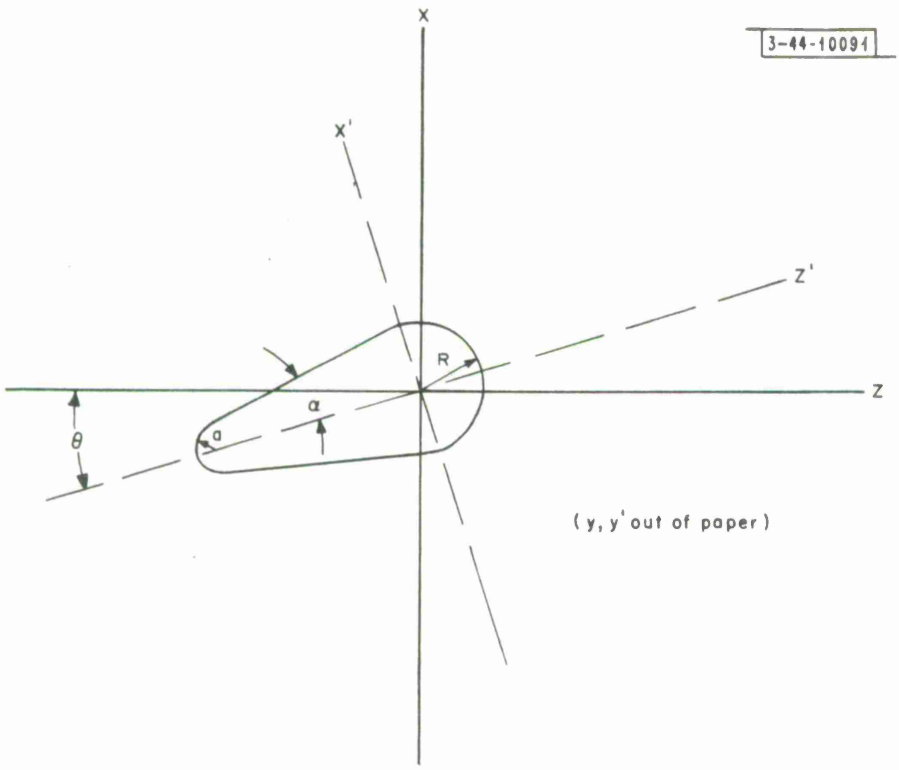

Fig. 2. Geometry for cone-sphere.

regions where d^3A/dz^3 is non-zero. For $\lambda \to 0$, the one wavelength pulse used to obtain Eq. (2.4) has the appearance of a doublet for which the scattered field is also proportional to d^3A/dz^3, as seen from Eq. (2.3). In the next section, we will calculate $A(z)$ for a cone-sphere as a function of target dimensions and aspect angle.

III. SCATTERING BY THE CONE-SPHERE

In this section we will calculate the response of a cone-sphere to an incident ramp waveform as a function of cone angle, aspect angle, sphere radius, and tip radius. This ramp response may then be used to obtain the scattered field, as discussed in the previous section. To calculate $A(z)$ for the cone-sphere, we use the coordinates shown in Fig. 2.

In the $x' - y' - z'$ coordinate system, the surface of the cone-sphere is given by

$$x'^2 + y'^2 = \begin{cases} a^2 - [z' + (R - a)\csc\alpha]^2 & ; \; -R\csc\alpha + a(\csc\alpha - 1) \le z' \le -R\csc\alpha + a\cos\alpha\cot\alpha \\ & \qquad \text{(tip)} \\ (z' + R\csc\alpha)^2\tan^2\alpha & ; \; -R\csc\alpha + a\cos\alpha\cot\alpha \le z' \le -R\sin\alpha \\ & \qquad \text{(cone)} \\ R^2 - z'^2 & ; \; -R\sin\alpha \le z' \le R \\ & \qquad \text{(sphere)} \end{cases} \tag{3.1}$$

where R and a are the sphere and tip radii and α is the cone half-angle. These equations may be converted to the $x - y - z$ coordinates through the transformation

$$\begin{aligned} x' &= x\cos\theta - z\sin\theta \\ y' &= y \\ z' &= x\sin\theta + z\cos\theta \end{aligned} \quad , \tag{3.2}$$

where θ is the aspect angle, to give

$$y^2 = -(x\cos\theta - z\sin\theta)^2 + \begin{cases} a^2 - [x\sin\theta + z\cos\theta + (R-a)\csc\alpha]^2 & ; \text{ tip} \\ (x\sin\theta + z\cos\theta + R\csc\alpha)^2 \tan^2\alpha & ; \text{ cone} \\ R^2 - (x\sin\theta + z\cos\theta)^2 & ; \text{ sphere} \end{cases} \qquad (3.3)$$

The tip-cone and cone-sphere joints are not planes of constant z but may be expressed in the form $x_1(z)$ and $x_2(z)$. The area of the cone-sphere at a fixed value of z is given by

$$A(z) = 2\int y(x, z)\, dx \quad . \qquad (3.4)$$

In general, this integral must be split into integrals over the tip, cone, and sphere, depending on the value of z. From Eq. (3.3), it is seen that y^2 is a quadratic function of x in each region and thus, the integrals in Eq. (3.4) may be done analytically. Depending on the values of c_1, c_2, and c_3, the integral, $\int (c_1x^2 + c_2x + c_3)^{1/2}\, dx$, is expressed in terms of various elementary functions. It should be noted that y^2 is not a quadratic function of x for an arbitrary body of revolution but only for bodies comprised of linear and quadratic surfaces.

In deriving $A(z)$, we have calculated the area of the cone-sphere intersecting the plane $z = \text{const}$ independent of whether this area is illuminated or shadowed. In the next section we will attempt to justify this neglect of shadowing, and through the introduction of creeping waves, will partially correct for the effects of shadow boundaries and surface waves.

IV. SHADOWING EFFECTS AND CREEPING WAVES

In obtaining the ramp response of the cone-sphere in the previous section, we used the total target area rather than the illuminated area. This is consistent with the version of physical optics used by Adachi[5] for slender bodies with no specularly reflecting points in the shadowed region. For the cone-sphere, however, such shadowed specular points are present for a range of aspect angles and will be dealt with later in this section.

Before continuing the discussion of shadowing for the present problem, it is appropriate to review its treatment in cw physical optics calculations. For nose-on incidence on a pointed cone-sphere, the integral in Eq. (2.1)

becomes

$$2\pi \left[\tan^2\alpha \int_{-R\csc\alpha}^{-R\sin\alpha} (z + R\csc\alpha)\exp(-2ikz)\,dz - \int_{-R\sin\alpha}^{z^*} z\exp(-2ikz)\,dz\right]$$

$$= \frac{\pi}{2k^2}\left[-\tan^2\alpha \exp(2ikR\csc\alpha) + \sec^2\alpha \exp(2ikR\sin\alpha)\right.$$

$$\left. - (1 + 2ikz^*)\exp(-2ikz^*)\right] \quad . \qquad (4.1)$$

The first term in this expression represents tip scattering, while the second term represents scattering from the cone-sphere joint. The term containing z^* should describe the effect of the rear termination but does not do so correctly. If the physical optics integral is cut off at the shadow boundary ($z^* = 0$), the last term in Eq. (4.1) describes a "joint" return from the shadow boundary. If the integral is extended over the entire target ($z^* = R$), then this term describes a "specular" return from the rear of the sphere. Clearly, neither of these techniques correctly describes the effect of the shadow boundary and of surface waves. The usual procedure[6] for dealing with this difficulty is to neglect the term containing z^* entirely and to replace it with a term describing creeping waves (obtained from the solution for a sphere). For a pulse waveform, this fictitious return occurs only for $0 \le \theta \le \pi/2 + \alpha$ and may be eliminated by using the expression $R^2 - z'^2$ for $z' \ge R$ in Eq. (3.1). This technique is successful as a consequence of the fact that the scattered field is proportional to the third difference (or derivative) of the target area.

After eliminating fictitious returns from the shadow region, it is necessary to include the creeping-wave return. The creeping-wave return at nose-on incidence is usually taken to be the same as that for a sphere of the same radius (with some slight corrections[7]). Since an exact calculation of the creeping wave even for a sphere[8] is fairly complicated, it will be necessary to use an approximate method to determine the cone-sphere creeping wave for non-zero aspect angles.

A model is presented in Appendix A, in which the creeping-wave return at aspect angle θ is given by the product of the nose-on creeping-wave return and a geometrical factor $F(\theta)$ given by Eqs. (A-6) and (A-7) and graphed in Fig. A-1,

$$F(\theta) = \begin{cases} 1 & ; \quad 0 \le \theta \le \alpha \\ 1 - 2\varphi^*/\pi & ; \quad \alpha \le \theta \le \pi/2 + \alpha \\ 0 & ; \quad \pi/2 + \alpha \le \theta \le \pi \end{cases} , \tag{4.2}$$

where

$$\cos^2\varphi^* = \begin{cases} \sin^2\alpha/\sin^2\theta & ; \quad \alpha \le \theta \le \pi/2 \\ (\sin^2\alpha - \cos^2\theta)/\sin^2\theta & ; \quad \pi/2 \le \theta \le \pi/2 + \alpha \end{cases} . \tag{4.3}$$

We must now calculate the creeping-wave return for nose-on incidence. For this purpose we make use of the empirical result[9] for a sphere of radius R,

$$\sigma_{cr} \approx \pi R^2 (kR)^{-5/2} \quad \text{for} \quad 1 \le kR \le 15 . \tag{4.4}$$

The amplitude of the scattered field varies as $k^{-5/4}$ and the phase is such that the creeping-wave ramp response (obtained using Fourier transforms) has the form

$$\text{Ramp}_{cr}(z) \approx \frac{\hat{\varepsilon}}{2\pi r} 6R^{-1/4}(z - \pi R/2)^{9/4} \tag{4.5}$$

The creeping wave given by Eqs. (4.2) and (4.5) must now be added to the previous ramp response given by Eq. (2.5) to obtain the scattered field.

In the following section, results obtained from the present model will be compared with cw measurements of cross section as a function of aspect angle and wavelength. This will provide a means of estimating the accuracy of this model.

V. NUMERICAL RESULTS AND COMPARISON WITH EXPERIMENT

A computer program has been written to calculate the backscattered field as a function of range given the cone half-angle, aspect angle, tip radius, base radius, wavelength, and pulse length (in wavelengths). Typical results are presented in Figs. 3a and 3b, which show the nose-on and tail-on scattering of a four-wavelength pulse. The tip, joint, creeping wave, and specular returns are evident and are seen to have differing waveforms. The specular return is similar to the incident pulse, while the joint return is proportional to the integral of the incident pulse. The tip return is the sum of specular and joint contributions and its detailed shape depends on a/λ. The creeping-wave return

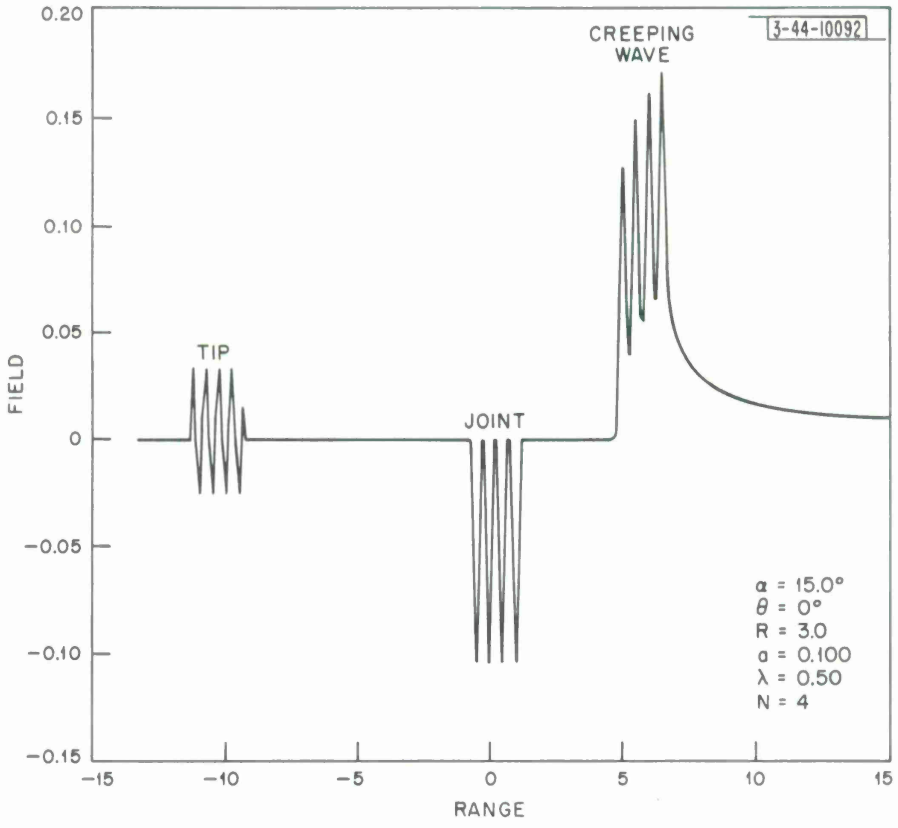

Fig. 3a. Scattered field for nose-on incidence on cone-sphere.

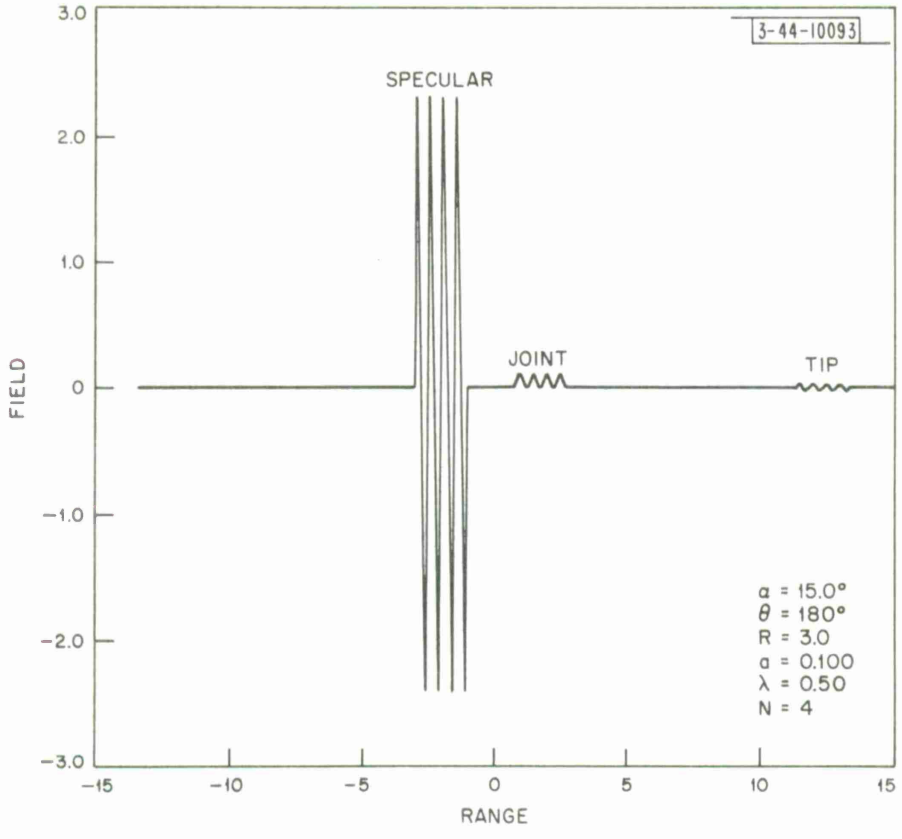

Fig. 3b. Scattered field for tail-on incidence on cone-sphere.

is seen to have a mean value which increases with time (range) until the pulse has passed.

To obtain agreement with known results, the cross section is defined in terms of the local amplitude of oscillation as follows:

$$\sigma = 4\pi r^2 \left| \text{scattered amplitude/incident amplitude} \right|^2 \quad . \qquad (5.1)$$

The amplitude is defined in terms of the difference between the maximum and minimum field values occurring within a half-wavelength of the point considered.

As the pulse length increases, more than one scattering center will contribute to the return, and interference may take place. Examples of this interference are shown in Fig. 4, where the contributing scattering centers are indicated. It is seen that the tip and joint interfere constructively, while the joint and creeping wave interfere destructively.

If the pulse is sufficiently long, all scattering centers will contribute to the scattered field over a certain range, and this cross section should equal the cw cross section of the target. Since the cw cross section of the cone-sphere has been measured for a variety of body parameters, it is of interest to compare these measurements with the results of the present model. In Fig. 5 the nose-on cross section is shown as a function of R/λ for the present model, for cw theory[10] and for several experiments. Figures 6a through 6d show the cross section as a function of aspect angle for the present model superimposed on experimental results.[10] In all these figures, the present results are in qualitative agreement with experiment, and the numerical deviations are usually of the order of a few db. These differences are comparable to the experimental differences between HH and VV polarization, and since the physical optics approximation predicts no polarization dependence for backscattering, we should not expect better agreement between the present model and experiment. The numerical results presented in Fig. 6a through 6d at 10° aspect-angle intervals approximate the average or smoothed cross-section pattern. To determine whether the detailed lobe structure could be obtained, the cross section was calculated every 1° from 30° to 60° for $R/\lambda = 1.45$ (see Fig. 6b). The fact that the correct lobe structure was not obtained may be understood if lobing is interpreted as interference between scattering centers.

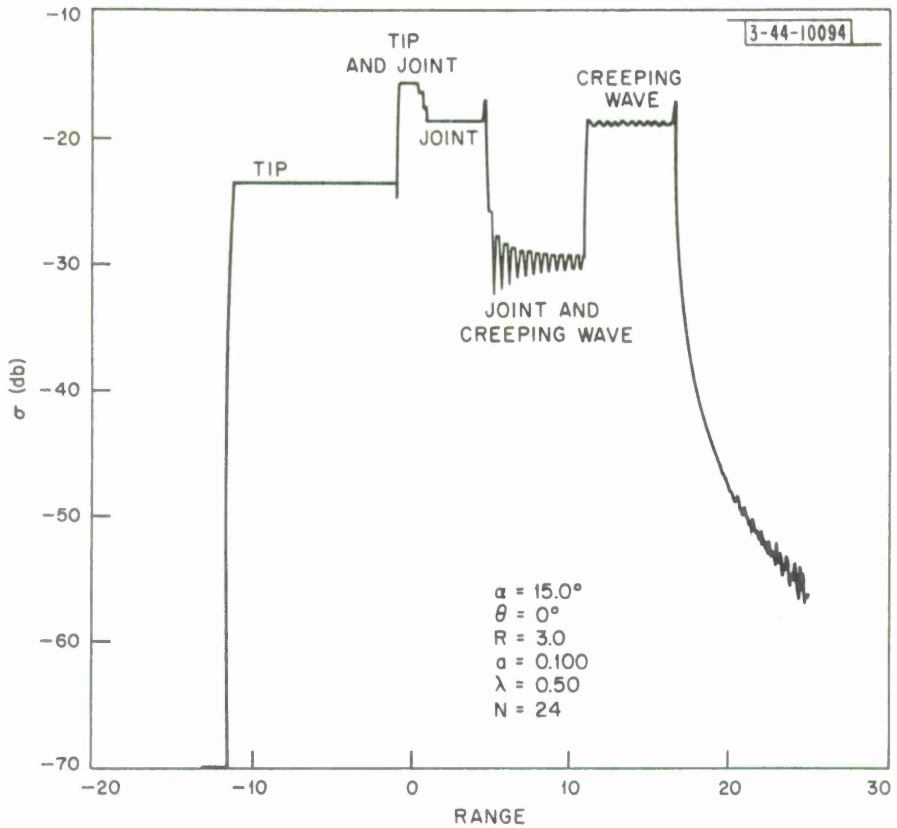

Fig. 4. Pulse response of cone-sphere showing interference between scatterers.

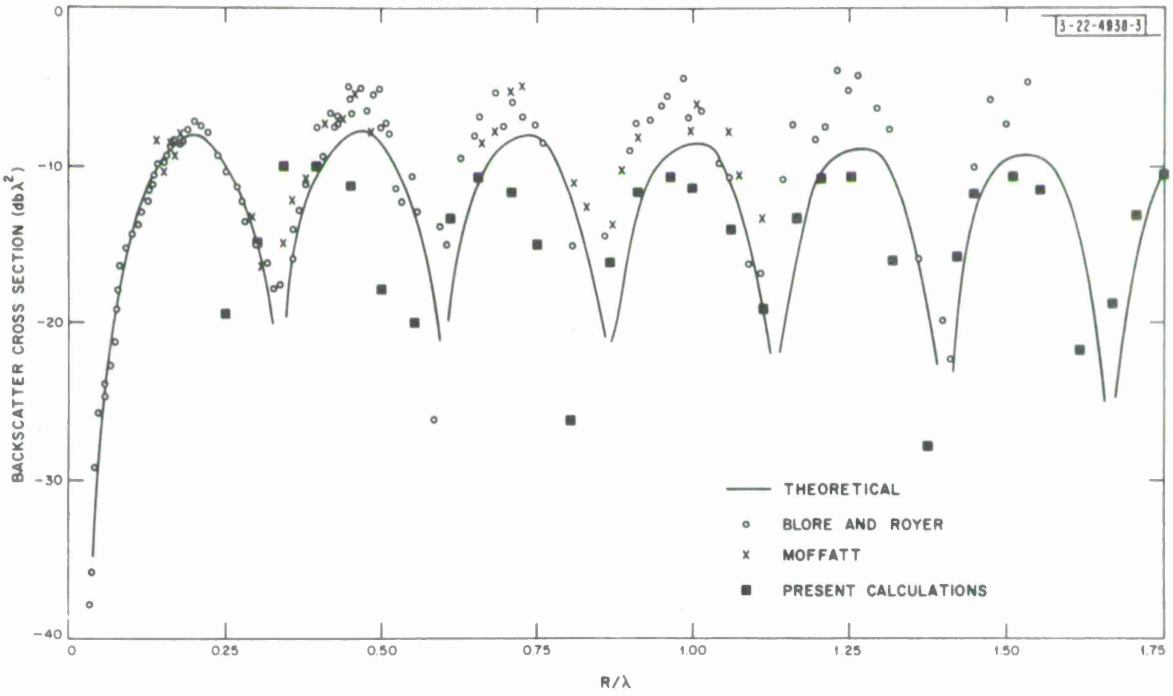

Fig. 5. Experimental and theoretical nose-on cross section of a 15° half-angle pointed cone-sphere.

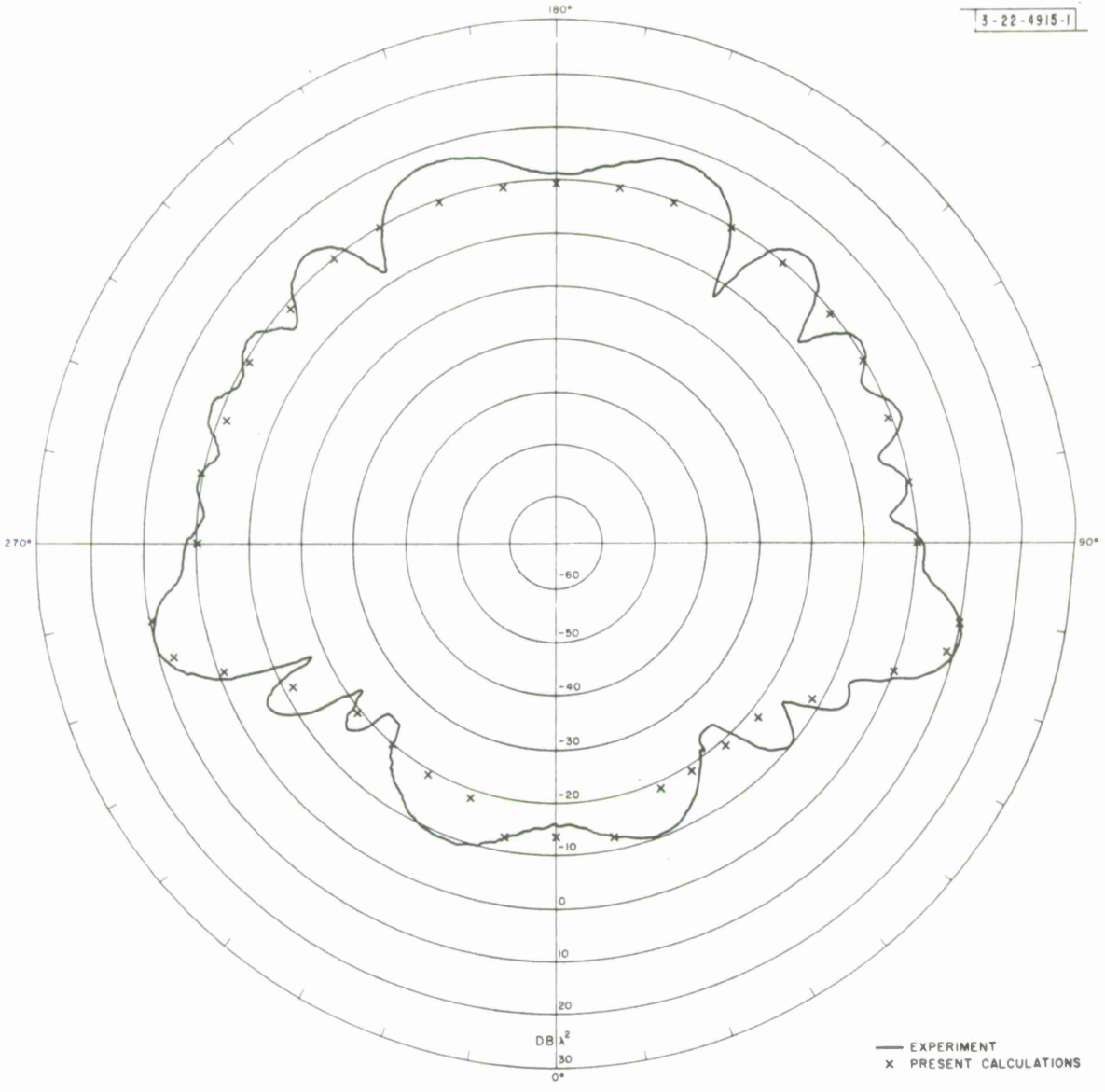

Fig. 6a. Calculated and measured (HH polarization) cross section; $\alpha = 12.5^{o}$, $R/\lambda = .6$.

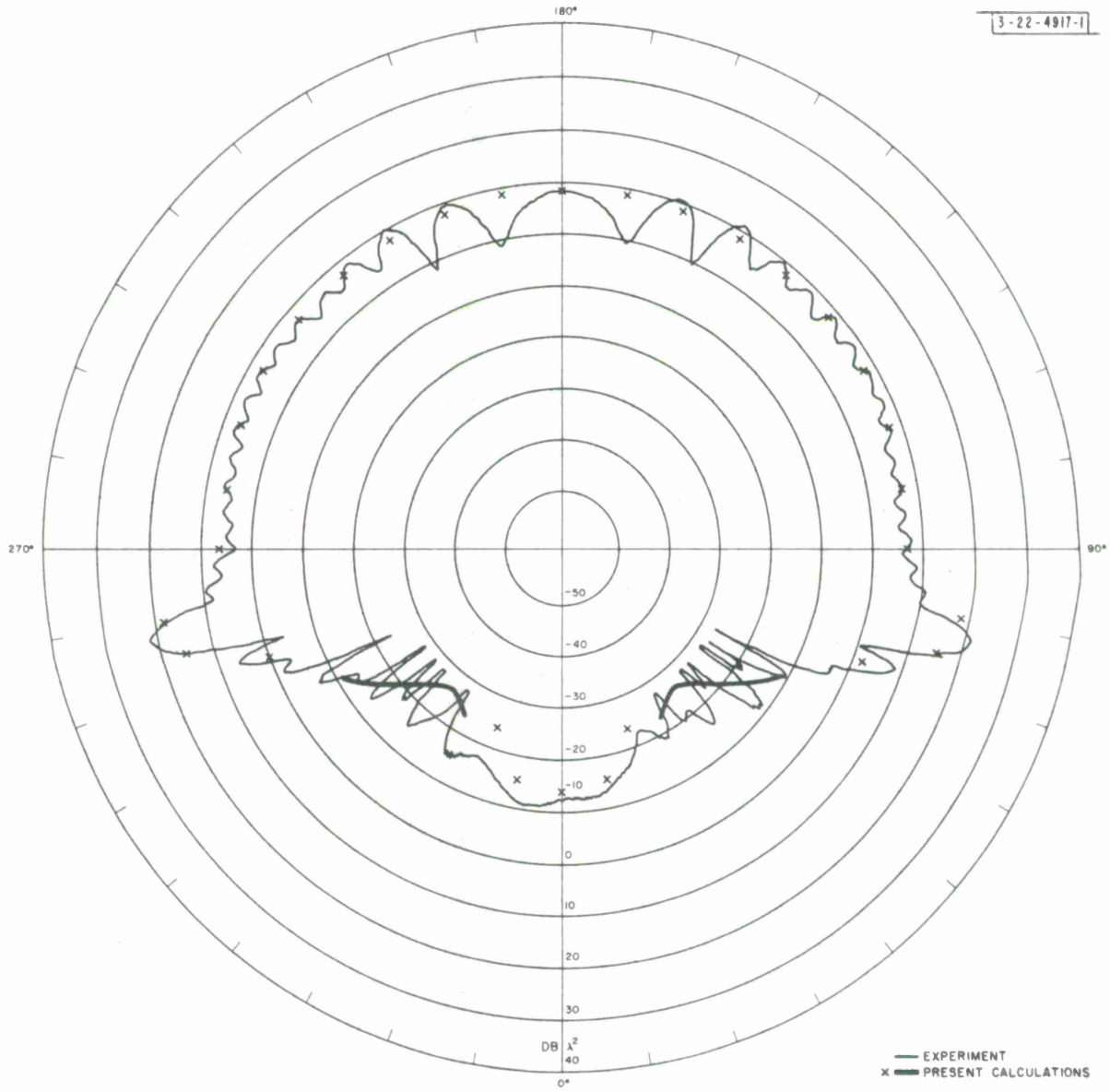

Fig. 6b. Calculated and measured (HH polarization) cross section; $\alpha = 12.5^{\circ}$, $R/\lambda = 1.45$.

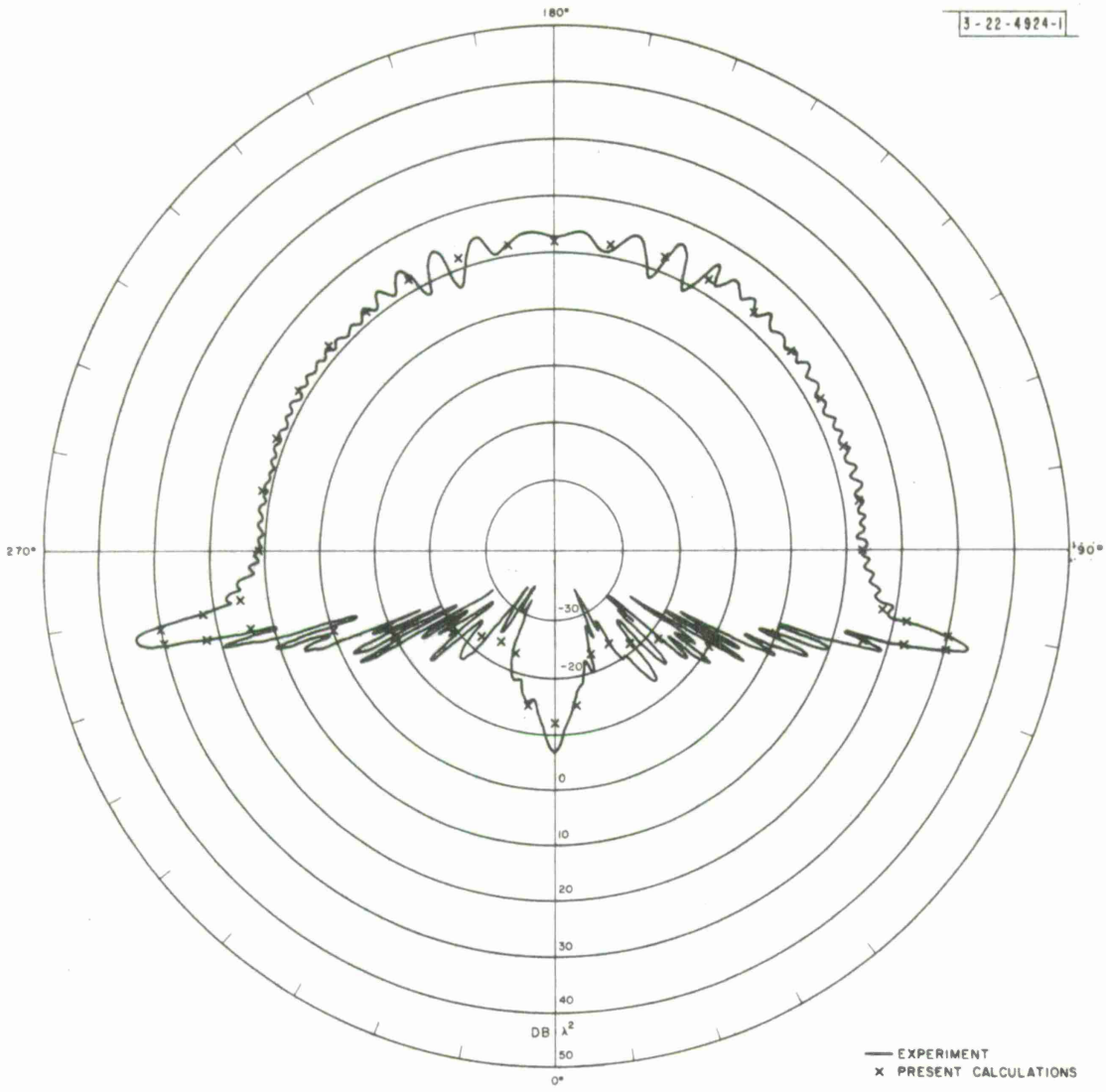

Fig. 6c. Calculated and measured (HH polarization) cross section; $a = 12.5^{\circ}$, $R/\lambda = 2.4$.

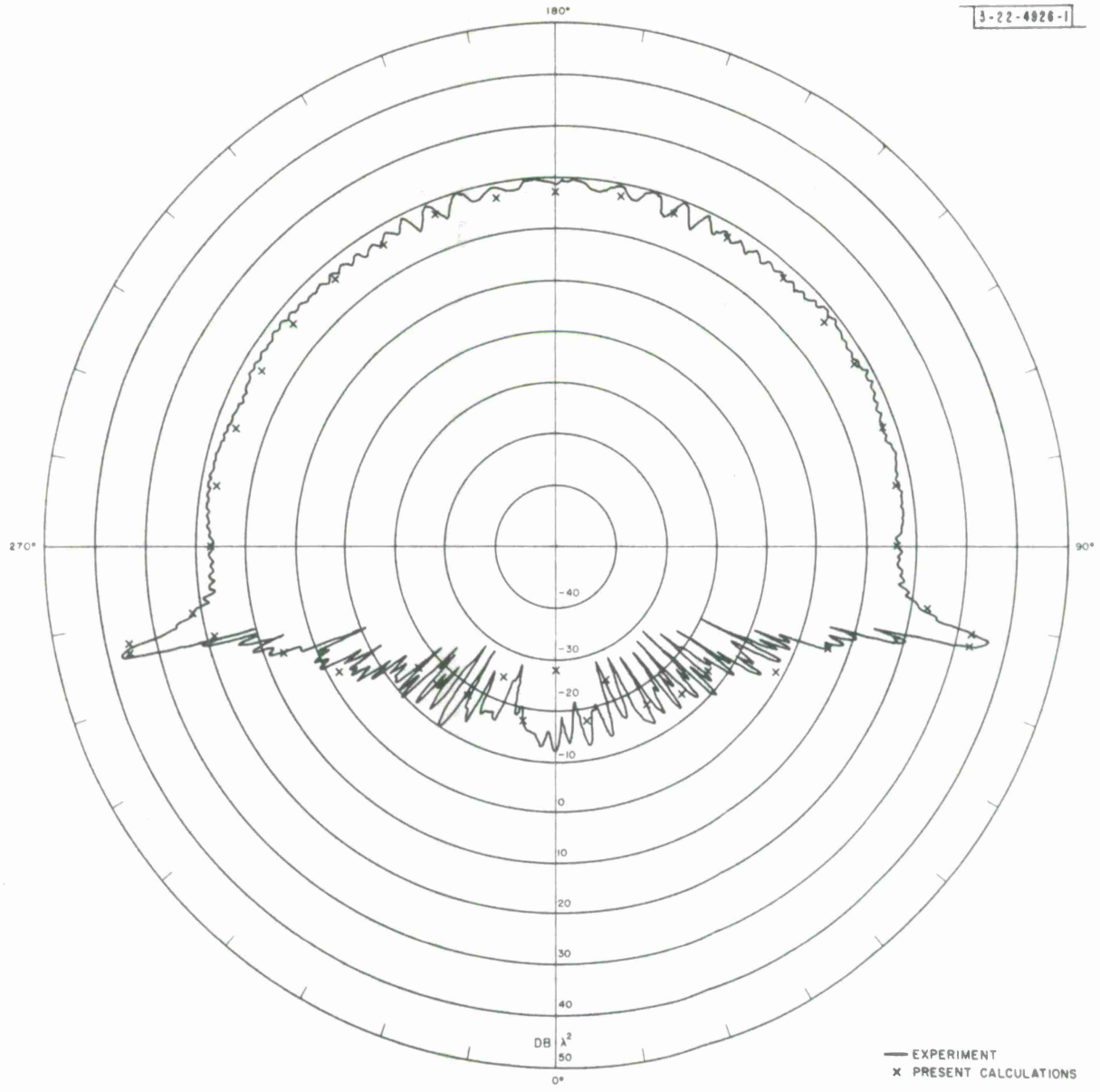

Fig. 6d. Calculated and measured (HH polarization) cross section; $a = 12.5^{o}$, $R/\lambda = 3.91$.

To obtain a good approximation to the average cross section, it is only necessary to represent the dominant scattering center fairly accurately. However, to obtain the correct lobe structure, it is necessary to represent all scattering centers very accurately.

VI. SCATTERING BY INDIVIDUAL CENTERS

Before investigating the scattering by individual scattering centers in detail, it is essential to identify these centers. In Figs. 3a and 3b the tip, joint, specular, and creeping-wave returns appear as localized scatterers for nose-on and tail-on incidence. At other aspect angles, these individual scattering centers may themselves show some structure. The specular return arises from the specular point (or line) on the target and should not have any structure regardless of aspect angle. Similarly, all rays contributing to the creeping-wave return have the same phase and will appear to come from a point scatterer. The joint return, however, is produced by a ring of radius $R \cos \alpha$ and the elements of this ring are all in phase only for nose-on and tail-on incidence. At arbitrary aspect angles, the returns from different parts of the ring will differ in phase, and these parts may be resolvable if the pulse is sufficiently short. In Figs. 7a and 7b, showing the scattering from a typical target at 0° and 30° aspect angles, the joint return is seen to separate into distinct returns from the leading and trailing edges of the ring. (The additional returns between the tip and joint are due to numerical round-off errors and provide an estimate of the accuracy of the calculations.) It is at these edges of the cone-sphere joint (points A and B in Fig. 8) that the ring is perpendicular to the direction of incidence. These scattering centers may also be identified using conventional cw physical optics by finding the points of stationary phase in Eq. (2.1).[11]

The tip scattering consists of a specular part and a return from the tip-cone joint. If the tip is sufficiently large, these will be resolvable and, for some aspect angles, the joint return will show structure similar to that of the cone-sphere joint. For the cases we will consider, however, the tip dimensions are fairly small and the tip appears as a single localized scatterer.

Now that we have located the various scattering centers, it is of interest to study their behavior as a function of wavelength and aspect angle. This is

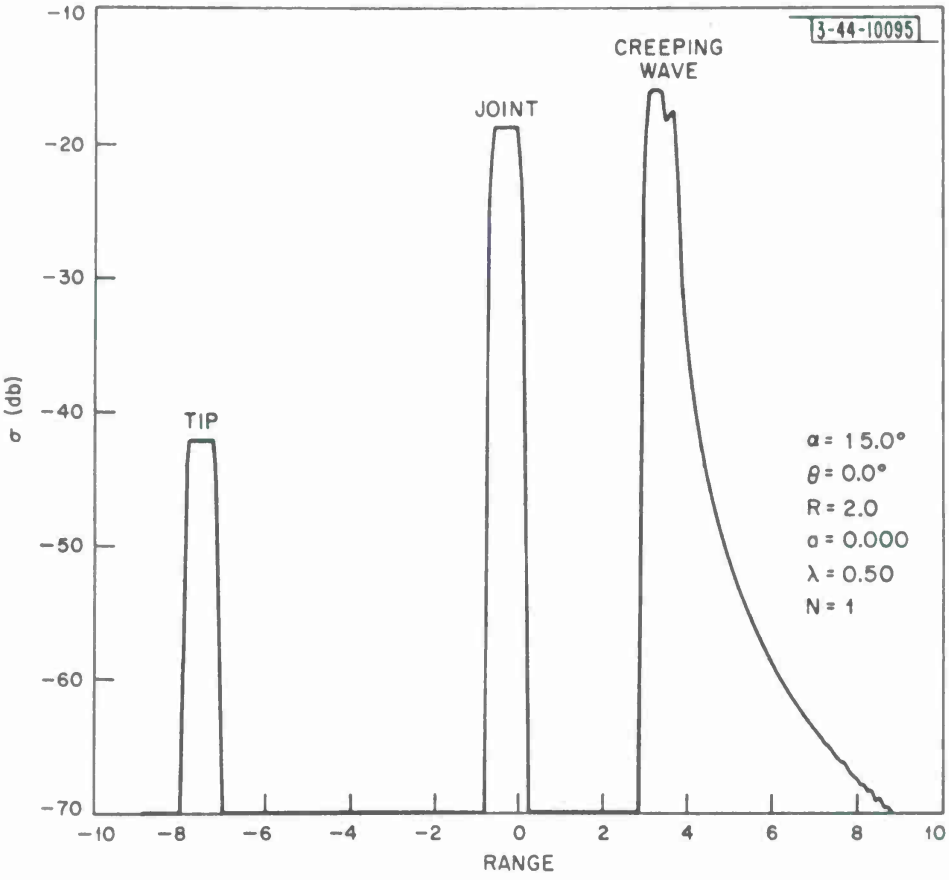

Fig. 7a. Scattering from a 15° half-angle cone-sphere at 0° aspect angle.

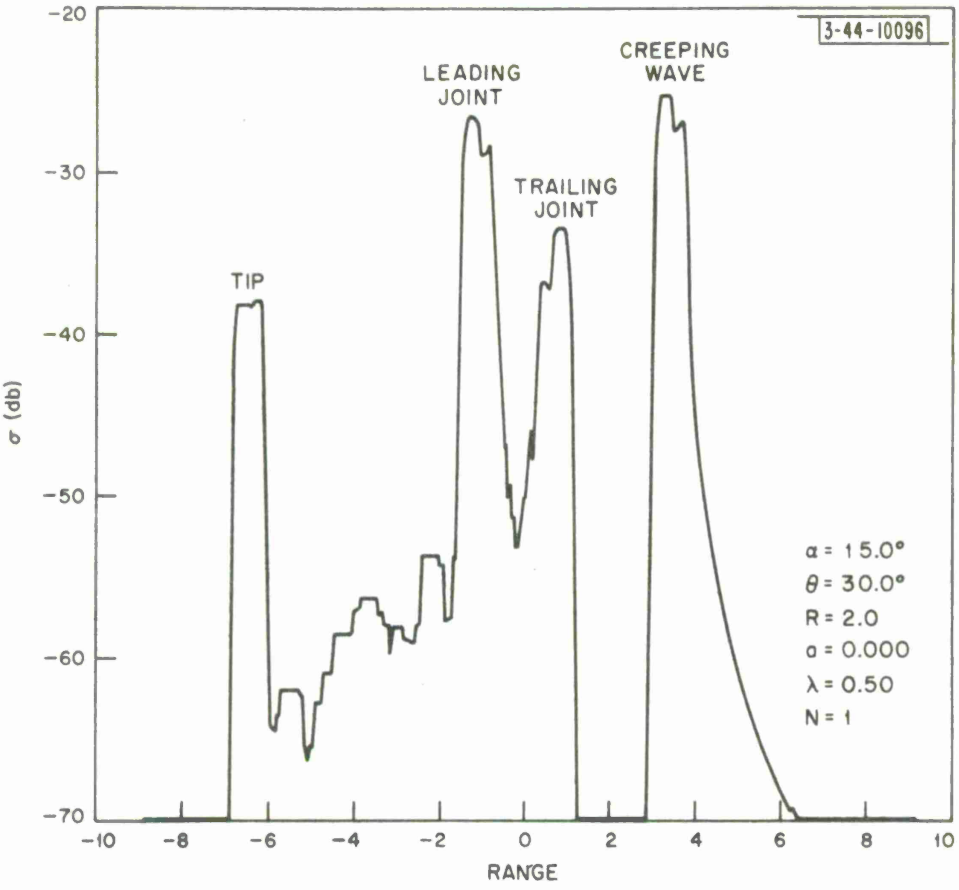

Fig. 7b. Scattering from a 15° half-angle cone-sphere at 30° aspect angle.

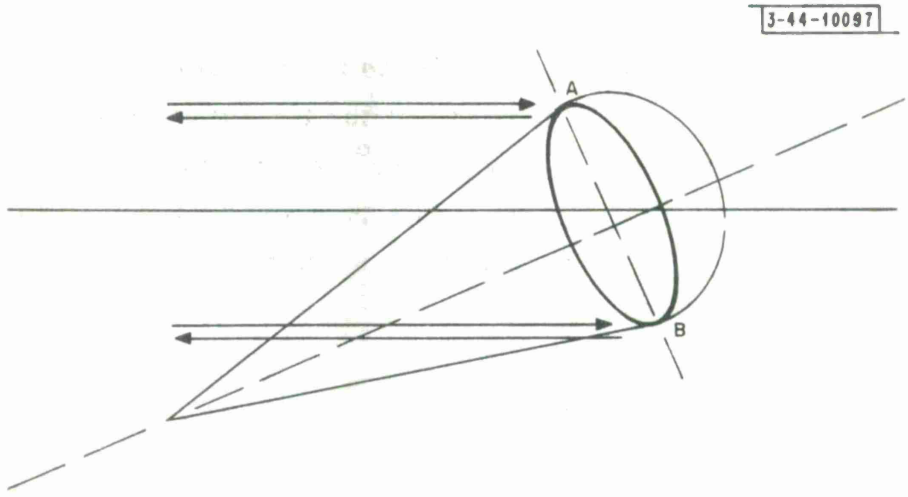

Fig. 8. Scattering centers on cone-sphere joint.

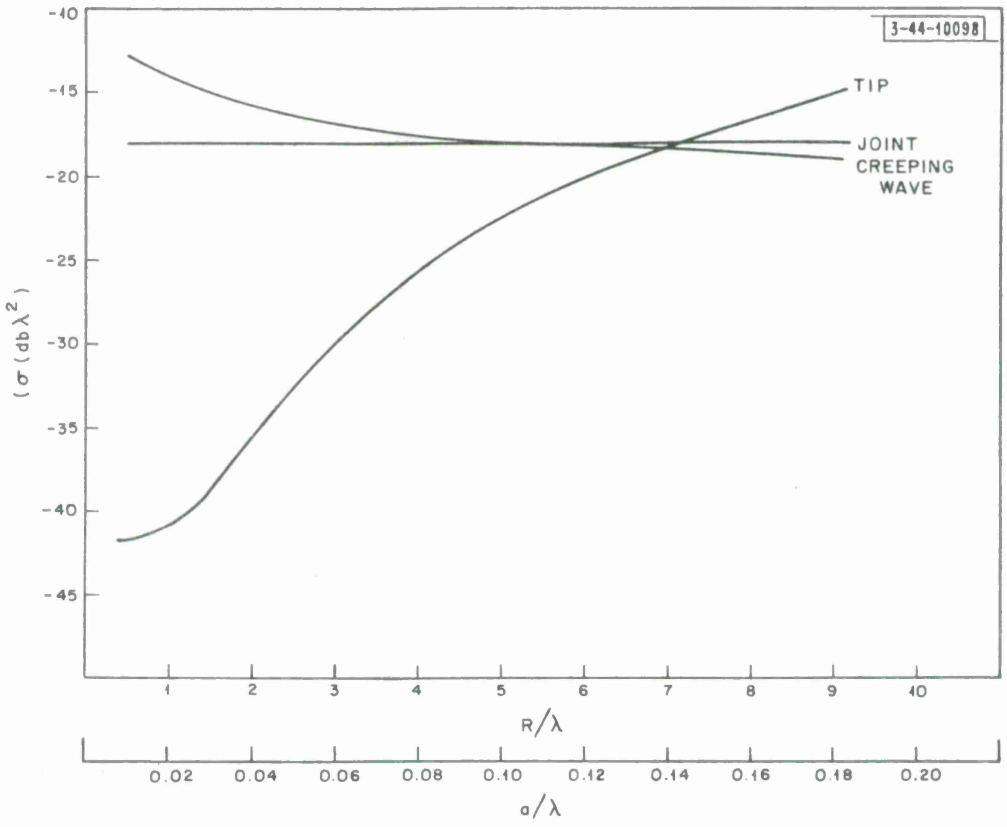

Fig. 9. Scattering centers at nose-on incidence; $\alpha = 15^{\circ}$.

done by using an incident pulse short enough to resolve individual centers. Figure 9 shows the nose-on cross sections of the tip, joint, and creeping-wave returns as functions of R/λ and a/λ for a 15° half-angle cone-sphere. For a fixed target size, the horizontal axis corresponds to a frequency axis. At low frequencies, the creeping-wave return exceeds the joint return and both are much larger than the tip return. As the frequency increases, however, the creeping wave becomes weaker, while the joint remains constant. The tip return increases and, at high frequencies, may provide the dominant contribution to the scattering.

In Fig. 10, the scattering from a 15° cone-sphere with $R/\lambda = 3$ and $a/\lambda = .06$ is shown as a function of aspect angle. The creeping wave is seen to be constant near nose-on and decreases monotonically as the aspect angle increases. The joint return decreases rapidly and divides into leading- and trailing-edge returns as θ increases from zero. These joint cross sections pass through minima and begin to increase as broadside incidence ($\theta = 75^{\circ}$) is approached. Near broadside the leading joint and specular returns run together and cannot be resolved. The tip return is roughly constant near nose-on and increases slowly as broadside is approached. For other values of R/λ or a/λ, the aspect-angle dependence of the tip and joint returns may differ from those shown in Fig. 10. The joint and tip returns for $\theta > 90^{\circ}$ are very similar to those for $\theta < 90^{\circ}$ due to the use of the physical optics approximation and the type of shadowing assumed. These returns for $\theta > 90^{\circ}$ are much weaker than the specular return, which is a maximum for broadside incidence and is a constant for incidence on the rear sphere. There are many other combinations of target size, shape, and orientation, which could be presented, but it is felt that this would add nothing essentially new to what is shown in Figs. 9 and 10.

It must be remembered that these results have been derived from an approximation to physical optics which is itself inexact. The fact that the present model shows good agreement with experiment (see Sec. V) indicates that the results for the individual scattering centers are probably correct, but errors of several db in cross section are to be expected.

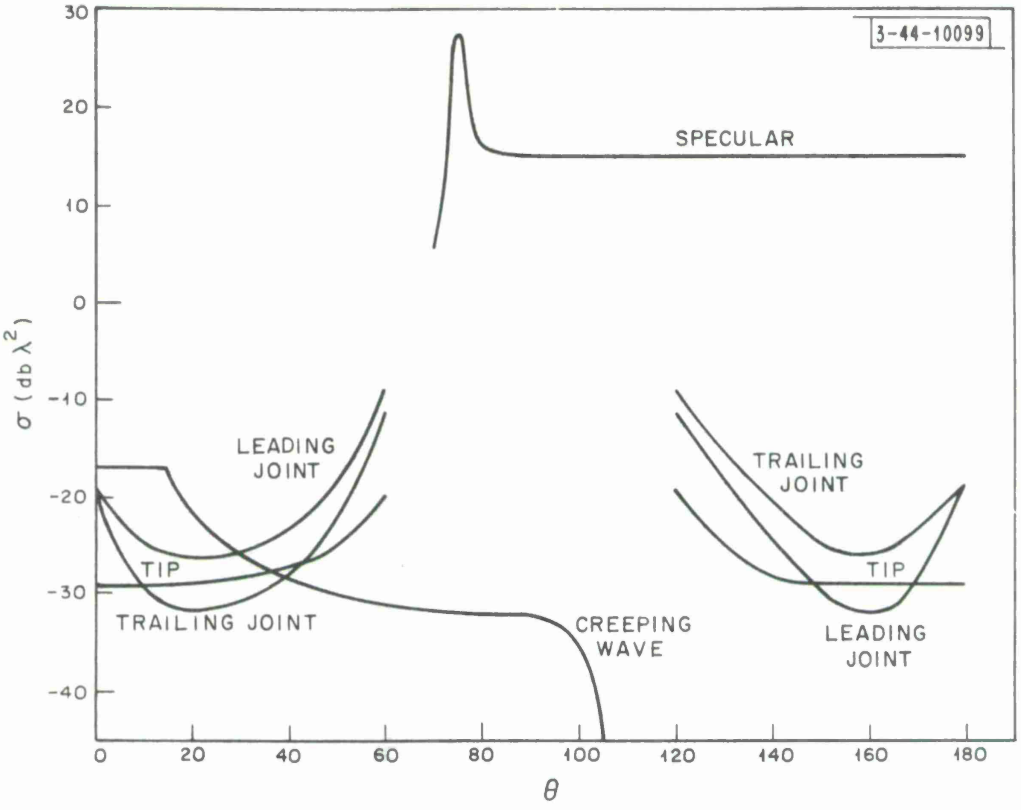

Fig. 10. Scattering centers as a function of aspect angle; $\alpha = 15^{o}$, $R/\lambda = 3$, $a/\lambda = .06$.

VII. CONCLUSIONS

At this point it is useful to summarize the present method and results. The scattering from a conducting cone-sphere is calculated using physical optics for an incident signal consisting of a pulse of triangular waves. Use of this waveform reduces the physical optics integrals to finite summations. In essence, we are approximating a sinusoid by a series of line segments. More refined models might use a larger number of segments to better approximate the sinusoid; in the limit, this is equivalent to numerical evaluation of the physical optics integrals.

The entire surface of the target (illuminated and shadowed) is assumed to contribute to the scattering, but fictitious returns are eliminated by a procedure analogous to that used in conventional physical optics calculations. Creeping waves are included by using the known results for a sphere with an aspect-angle dependence obtained from a ray-tracing model.

If the pulse length is sufficient to illuminate the entire target simultaneously, the cross section obtained should equal the cw cross section. Calculated and measured results show agreement for a variety of cases. It should be noted that this agreement implies only that the return from the dominant scattering center is represented accurately. In particular, for incidence on the rear sphere, the specular return is much stronger than any other return, and the agreement between the present model and experiment does not insure that these additional returns are described correctly. However, in the region near nose-on, this agreement indicates that the present results are not grossly in error. For short-pulse incidence, the scattering may consist of tip, leading-joint, trailing-joint, creeping-wave, and specular returns. These various returns have been studied as a function of the target parameters.

It is of interest to consider other target shapes for which this method is applicable. The calculation of $A(z)$ from Eq. (3.4) constitutes the solution to the problem, and this integral is considerably simpler than the physical optics integral Eq. (2.1). In particular, for bodies of revolution formed from linear and quadratic curves, $A(z)$ may be evaluated explicity. This class of bodies includes those comprised of portions of spheres, cones, cylinders, paraboloids,

spheroids, hyperboloids, etc. For many targets, however, there will be a problem in describing returns such as the creeping wave on a cone-sphere or the diffracted wave on a flat-backed cone. These returns are not obtainable from physical optics and must be included separately to adequately describe the scattering. If this is done, the present method may prove useful for a variety of targets.

SDW:cm

APPENDIX A

A Model of Creeping Waves for the Cone-Sphere

This appendix serves to present a simple model which permits estimation of the creeping-wave return at any aspect angle. The geometrical theory of diffraction has been used to describe surface waves[12] and we will make use of its assumptions that the various rays contributing to the total field do not interact. A "creeping ray" which makes one circuit of the spherical part of the cone-sphere traces the same ray path as a creeping ray on an equivalent sphere, and should have the same contribution to the creeping wave return (if rays which loop the sphere more than once are neglected). For a sphere, the creeping rays encounter no obstacles in looping the sphere. For a cone-sphere, however, for some aspect angles, many creeping rays will intersect the cone-sphere joint and their paths will be considerably altered. As a first approximation, we will assume that any creeping ray which intersects the joint does not contribute to the creeping-wave return, thus neglecting the effect of creeping waves on the conical surface.

The basic assumption of the present model is expressed in Eq. (A. 1):

$$A_{cr}(\text{cone-sphere}) = A_{cr}(\text{sphere})\,(\text{fraction of contributing creeping rays}) \qquad \text{(A. 1)}$$

or

$$A_{cr}(\theta) = A_{cr}(0)\, F(\theta) \quad ,$$

where A_{cr} is the creeping-wave amplitude. This approximation should be fairly good since all contributing creeping rays have the same phase. To calculate $F(\theta)$ easily, we use the $x - y - z$ coordinate system of Fig. 2 and introduce the polar angle, ψ, and azimuthal angle, φ, about the z-axis.

Since the creeping rays propagate along great circles, all rays which contribute to the backscattered wave must pass through the anti-specular point ($\psi = 0$). A particular creeping-ray path is given by $\varphi = \varphi_i$ for ψ decreasing from $\pi/2$ to 0, and $\varphi = \varphi_i + \pi$ for ψ increasing from 0 to $\pi/2$. If this ray is to contribute to the creeping-wave return, it may not intersect the cone-sphere

joint. To determine which rays contribute, it is necessary to express the locus of points on the joint in the present coordinate system. This is done by noting that the line from the origin to any point on the joint makes an angle of $\pi/2 + \alpha$ (measured from the rear of the sphere) with the cone-sphere axis. Specifying an arbitrary point on the joint by (ψ, φ) and the point of the rear of the sphere by $(\psi_1 = \theta,\ \varphi_1 = 0)$, and using spherical trigonometry we find

$$\cos\psi\cos\theta + \sin\psi\sin\theta\cos\varphi + \sin\alpha = 0 \quad . \tag{A.2}$$

This may be solved to find the equation of the cone-sphere joint, $\psi = \psi(\varphi)$, for a given aspect angle θ and half-angle α.

It is now necessary to use these results to find $F(\theta)$, as defined in Eq. (A.1). Rays will be incident on the cone-sphere at all values of azimuth φ_i. We must determine the ranges of φ_i for which the creeping-ray paths $(\varphi = \varphi_i,\ \varphi_i + \pi,\ \psi \le \pi/2)$ intersect the cone-sphere joint $\psi = \psi(\varphi)$. More explicitly, we must find the range of φ_i for which either $\psi(\varphi_i)$ or $\psi(\varphi_i + \pi)$ is less than $\pi/2$. Defining $x = \cos\psi$, Eq. (A.2) becomes

$$x^2(\cos^2\theta + \sin^2\theta\cos^2\varphi) + x(2\cos\theta\sin\alpha) + (\sin^2\alpha - \sin^2\theta\cos^2\varphi) = 0 \quad , \tag{A.3}$$

or

$$Ax^2 + Bx + C = 0 \quad .$$

Non-contributing rays will have $x(\varphi_i)$ or $x(\varphi_i + \pi)$ between 0 and 1. Using the solution to the general quadratic equation, we will examine the conditions under which a ray is non-contributing. Since A is always positive, we must consider only two cases depending on the sign of B:

Case 1

$$B > 0\ (\theta < \pi/2) : 1 \ge x \ge 0 \quad \text{implies} \quad C \ge 0$$

or

$$\cos^2\varphi \ge \frac{\sin^2\alpha}{\sin^2\theta} \quad , \tag{A.4a}$$

Case 2

$$B < 0\ (\theta > \pi/2) : 1 \ge x \ge 0 \quad \text{implies} \quad B^2 - 4AC \ge 0$$

or

$$\cos^2\varphi \ge \frac{\sin^2\alpha - \cos^2\theta}{\sin^2\theta} \quad . \tag{A.4b}$$

Those rays for which $\cos^2\varphi_i$ satisfies inequalities (A.4a) and (A.4b) are non-contributing. If we introduce φ^* as that value of φ satisfying the equality sign in Eqs. (A.4a) and (A.4b), then the range of φ_i may be divided as follows:

$$\begin{aligned} &0 \le \varphi_i \le \varphi^* && \text{non-contributing rays} \\ &\varphi^* < \varphi_i < \pi - \varphi^* && \text{contributing rays} \\ &\pi - \varphi^* \le \varphi_i \le \pi && \text{non-contributing rays} \\ &\text{etc.} \end{aligned} \tag{A.5}$$

However, for many combinations of θ and α, there is no solution for φ^*. From Eq. (A.4a) we see that for $\theta < \alpha$, no rays are non-contributing and $F = 1$. From Eq. (A.4b) for $\theta > \pi/2 + \alpha$, all rays are non-contributing and $F = 0$. Thus, our results may be summarized by

$$F(\theta) = \begin{cases} 1 & 0 \le \theta \le \alpha \\ 1 - 2\varphi^*/\pi & \alpha \le \theta \le \pi/2 + \alpha \\ 0 & \pi/2 + \alpha \le \theta \le \pi \end{cases}, \tag{A.6}$$

where

$$\cos^2\varphi^* = \begin{cases} \sin^2\alpha/\sin^2\theta & \alpha \le \theta \le \pi/2 \\ (\sin^2\alpha - \cos^2\theta)/\sin^2\theta & \pi/2 \le \theta \le \pi/2 + \alpha \end{cases}. \tag{A.7}$$

The function $F(\theta)$ obtained from Eqs. (A.6) and (A.7) is shown in Fig. (A.1) for a variety of aspect angles.

The determination of $F(\theta)$ serves to reduce the problem of finding the creeping-wave amplitude for a cone-sphere at any aspect angle to that of finding the creeping-wave amplitude for a sphere (at least to this degree of approximation).

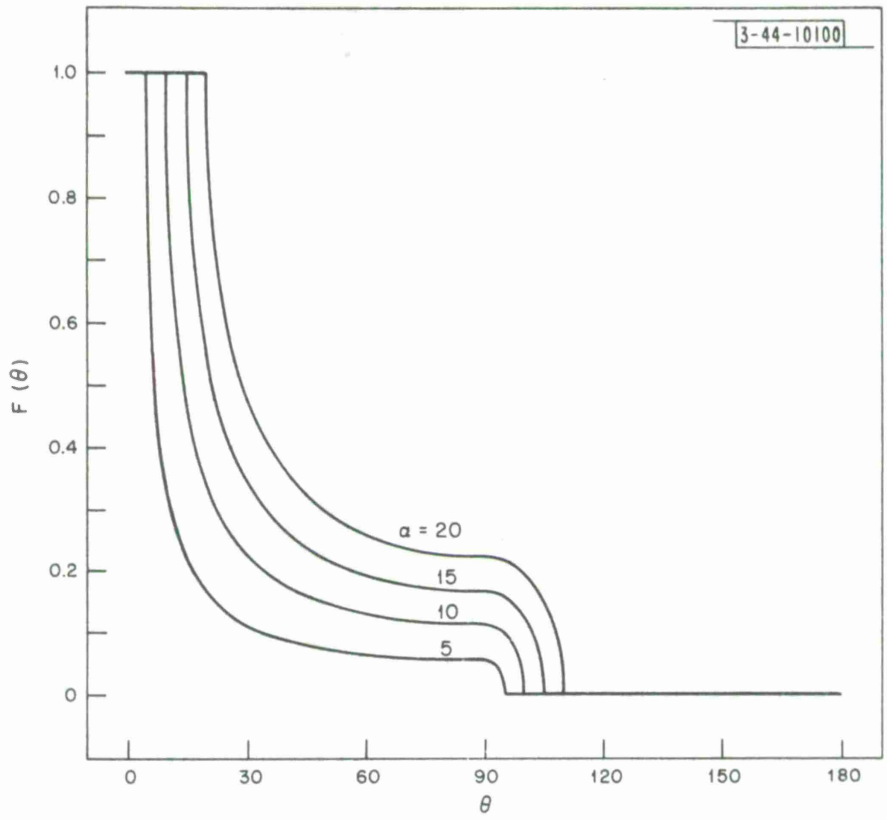

Fig. A-1. Geometrical factor for creeping waves.

References

1. See, for example, D. E. Kerr, ed., Propagation of Short Radio Waves, McGraw Hill, New York, p. 463 (1951).
2. S. D. Weiner and S. L. Borison, "Radar Scattering from Blunted Cone Tips," IEEE Trans. on Ant. and Prop., (to be published).
3. E. M. Kennaugh and R. L. Cosgriff, "The Use of Impulse Response in Electromagnetic Scattering Problems," IRE Nat. Conv. Rec., Pt. I, pp. 72-77,(1958).
4. E. M. Kennaugh and D. L. Moffatt, "On the Axial Echo Area of the Cone-sphere Shape," Proc. IEEE, 50, p. 199, (1962), and 51, p. 232, (1963).
5. S. Adachi, "The Nose-on Echo Area of Axially Symmetric Thin Bodies Having Sharp Apices," Proc. IEEE, 53, pp. 1067-1068, (1965).
6. See, for example, R. E. Kleinman and T. B. A. Senior, "Studies in Radar Cross Sections XLVIII - Scattering and Diffraction by Regular Bodies - II: The Cone," Univ. of Mich. Rad. Lab. Scientific Report No. 5,(Jan. 1963).
7. T. B. A. Senior, "The Backscattering Cross Section of a Cone-Sphere," IEEE Trans. on Ant. and Prop. AP-13, pp. 271-277 (March 1965).
8. T. B. A. Senior and R. F. Goodrich, "Scattering by a Sphere," Proc. IEE, 111, pp. 907-916, (May 1964).
9. J. W. Crispin, Jr. and A. L. Maffett, "Radar Cross-Section Estimation for Simple Shapes," Proc. IEEE, 53, pp. 833-848, (1965).
10. J. H. Pannell, J. Rheinstein, and A. F. Smith, "Radar Scattering from a Conducting Cone-Sphere," Lincoln Laboratory, M.I.T. Technical Report 349, (March 1964).
11. See, for example, S. Silver, ed., Microwave Antenna Theory and Design, McGraw Hill, New York, p. 119, (1949).
12. B. B. Levy and J. B. Keller, "Diffraction by a Smooth Object," Comm. Pure and Appl. Math. XII, pp. 159-209, (1959).

DISTRIBUTION

Group 22

J. H. Pannell

J. Rheinstein

A. F. Smith

Division 4

J. Freedman

Group 41

S. L. Borison (3)

D. L. Clark (5)

S. D. Weiner (3)

Group 42

A. A. Galvin

Group 43

R. C. Butman

Group 44

C. Blake

Group 45

S. J. Miller

Group 46

C. W. Jones

DOCUMENT CONTROL DATA – R&D

(Security classification of title, body of abstract and indexing annotation must be entered when the overall report is classified)

1. ORIGINATING ACTIVITY *(Corporate author)*
Lincoln Laboratory, M.I.T.

2a. REPORT SECURITY CLASSIFICATION
Unclassified

2b. GROUP
None

3. REPORT TITLE
A Model of Radar Scattering from the Cone-Sphere

4. DESCRIPTIVE NOTES *(Type of report and inclusive dates)*
Technical Note

5. AUTHOR(S) *(Last name, first name, initial)*
Weiner, Stephen D.

6. REPORT DATE
20 October 1966

7a. TOTAL NO. OF PAGES
36

7b. NO. OF REFS
12

8a. CONTRACT OR GRANT NO.
AF 19(628)-5167

b. PROJECT NO.
ARPA Order 498

c.

d.

9a. ORIGINATOR'S REPORT NUMBER(S)
Technical Note 1966-47

9b. OTHER REPORT NO(S) *(Any other numbers that may be assigned this report)*
ESD-TR-66-550

10. AVAILABILITY/LIMITATION NOTICES
Distribution of this document is unlimited.

11. SUPPLEMENTARY NOTES
None

12. SPONSORING MILITARY ACTIVITY
Advanced Research Projects Agency, Department of Defense

13. ABSTRACT

A technique is presented for calculating the radar cross section of a conducting cone-sphere as a function of cone angle, aspect angle, tip radius, base radius, and wavelength for both cw and short-pulse incident signals. A modification of the physical optics approximation is used in which the incident sinusoidal wave is replaced by finite summations. Creeping waves are included by using the known results for a sphere combined with an aspect-angle dependence obtained from a ray-tracing model. For long incident pulses, the calculated cross sections show good agreement with cw measured values. For short incident pulses, the behavior of individual scattering centers may be studied as a function of the target parameters.

14. KEY WORDS
radar scattering
electromagnetic scattering
radar cross section calculations